A fast Fourier transform micromechanical upscaling method for the study of the thermal expansion of a TATB-based pressed explosive

Andrey Ambos, Hervé Trumel, François Willot, Dominique Jeulin, Maxime Biessy

A fast Fourier transform micromechanical upscaling method for the study of the thermal expansion of a TATB-based pressed explosive

Andrey Ambos[†], Hervé Trumel[‡], François Willot[†], Dominique Jeulin[†], and Maxime Biessy[‡]

[†]MINES ParisTech, PSL - Research university, CMM - Centre for mathematical morphology
35, rue St Honoré, F-77300 FONTAINEBLEAU, France
[‡]CEA, DAM, Le Ripault, F-37260 MONTS, France

Abstract.
This paper presents the first phase of development of a multiscale numerical method operating at the microstructureal level for a TATB-based pressed plastic-bonded explosive. It uses a virtual model of microstructure mimicking the grain size distribution of the actual material, and a Fourier-based numerical scheme. At present, the method works with simplified microstructure and linear anisotropic thermoelastic behavior for the constituents. Neglecting the inter-granular binder leads to fairly overestimated values for isotropic elastic moduli and volumetric coefficient of thermal expansion. A first attempt to include the binder yielded much more realistic predictions for elastic moduli, but not for the volumetric thermal expansion coefficient. The origin of this discrepancy is thought to lie in the behavior of constituents.

Introduction

The quasi-static thermo-mechanical behavior of TATB-based pressed plastic-bonded explosives is complex, irreversible and highly nonlinear. Progressive damage occurs under quasi-static mechanical loading, and slow thermal loads induce irreversible dilation[1, 2], often referred to as "ratchet growth".

These phenomena are still not well understood, but involve necessarily sub-macroscopic processes, such as grain plasticity, microcracking or debonding. The first sub-macroscopic level is the so-called "mesoscopic" one, at which the individual grains, micro-cracks and grain boundaries become distinct objects, but remain considered as homogeneous objects. This level, which will be referred to as the "microstructure level" in the sequel, is roughly that of optical microscopy.

The present work is the first step of the development of a thermo-mechanical computational method operating at the microstructural level, the objective of which is to link the macroscopic response to the constituents' arrangements and behaviors, in other words a numerical homogenization method.

Such a tool requires (i) a geometrical description of the microstructure, (ii) a computational method, and (iii) constitutive models for the constituents and interfaces.

As no 3D microstructure imaging is available to date for the material described below, the method will rely on virtual models of microstructure. The FFT-based upscaling method will be chosen, as it

requires no meshing, and is not computationally demanding. Finally, this first phase of development will be performed in the framework of linear thermoelasticity, homogeneous temperature fields (slow thermal loads) and simplified microstructure.

The studied material

The material considered in the present work is a TATB-based pressed plastic-bonded explosive, containing less than 5% of an amorphous polymeric binder. The TATB powder is first coated by the binder in a slurry process, then dried and granulated, yielding about 1 mm diameter prills. The latter are then isostatically pressed at 200 MPa and moderate temperature.

The resulting solid material is relatively easy to polish using a standard metallographic-like procedure, and allows optical microscopy (reflected polarized light) observations[3, 4] to be carried out (Fig. 1). The microstructure is characterized by a coarse (millimetric) scale representing the vestigial prills (hollow white arrows in Fig. 1) and the finer scale of TATB grains. The latter contain several kinds of flaws, namely binder-filled voids (thin white arrows in Fig. 1), deformation bands (white arrows) and some rare micro-cracks (hollow black arrows). At this scale, the presence of inter-granular binder cannot be detected.

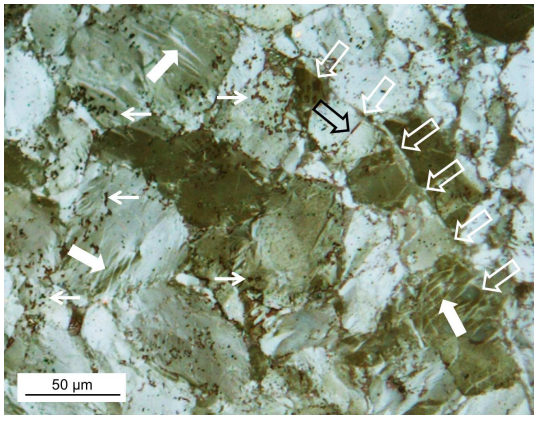

Fig. 1. Optical micrograph (polarized reflected light, enhanced contrast).

At room temperature and pressure, the Young's modulus of this material is 7.1 GPa, and its Poisson's coefficient is 0.335. Fig. 2 displays a typical result obtained with a linear dilatometer on a 5×5×50 mm sample submitted to ±10°C per hour thermal cycles. The response is highly nonlinear, and seemingly correlated with the glass transition, estimated at 104°C for this heating-cooling rate. In the glassy regime, around room temperature, the volumetric thermal expansion coefficient is 1.62×10^{-4} K^{-1}, which is almost half that of the TATB single crystal[5]. Strong local self-balanced stresses must develop upon heating, to counterbalance thermal strains. Upon reaching the glass transition, the rubbery binder is likely to deform easily, hence releasing internal stresses, no more hindering thermal expansion. The volumetric thermal expansion coefficient above the glass transition is 3.1×10^{-4} K^{-1}, slightly higher than that of the crystal.

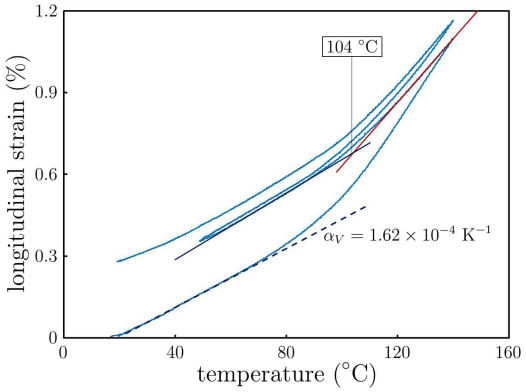

Fig. 2. Example of dilatational response under cyclic slow thermal loading.

Virtual microstructure generation

As optical microscopy provides quite complex pictures (see Fig. 1), a large SEM image is taken on a polished sample, after etching the surface by a suitable solvent of the binder to reveal grain boundaries. This image is then binarized and segmented, as illustrated in Fig. 3.

As is often done to approximate polycrystalline microstructures, a 3D space tessellation model will be sought[6], and its parameters will be identified by matching the 2D grain-size distribution measured in Fig. 3. The simplest one, namely the Poisson-

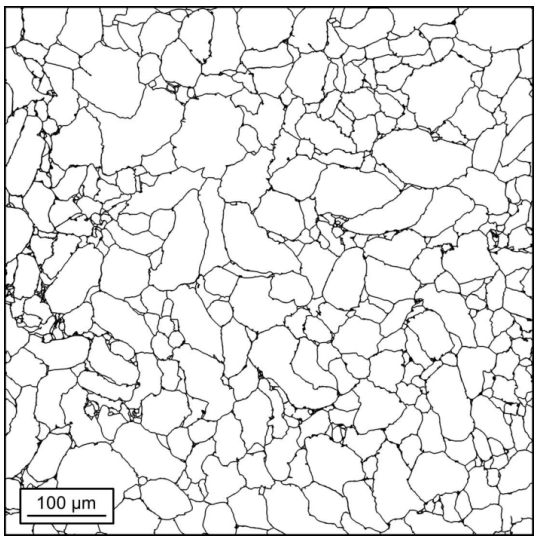

Fig. 3. Segmented image displaying the polycrystalline microstructure.

Voronoi tessellation, considers a Poisson distribution of seeds. The seeds appear simultaneously, and all grains grow from these seeds at the same isotropic growth rate. Any grain labeled k is defined as the set of voxels x for which:

$$d(x, c_k) \leq d(x, c_j), j \neq k \quad (1)$$

where $d(x, c_n)$ is the Euclidean distance between x and the seed of grain n. This model has only one parameter, namely the intensity of the Poisson process, i.e. the (statistical) average density of seeds per unit volume. For a given value of this parameter, a tessellation is generated, from which 2D cuts are selected, and grain size distributions are determined by morphological opening. The difference between such 2D grain size distributions and the one measured on the image of Fig. 3 is then minimized by varying the parameter of the model. The result, displayed in Fig. 4, shows that the Poisson-Voronoi model is unable to reproduce the 2D granulometry of the real material.

A more flexible model is therefore required. The Johnson-Mehl[7] one is characterized by a non-simultaneous nucleation process. In its simplest version, nucleation times follow a Poisson process. In order to obtain a model reproducing the experimental 2D grain size distribution, the nucleation process must be further refined, by making the nucleation rate to increase linearly with time. An example of generated microstructure is given in Fig. 5. Notice that the Johnson-Mehl tessellation has the definitive advantage of providing curved grain boundaries over the Voronoi one.

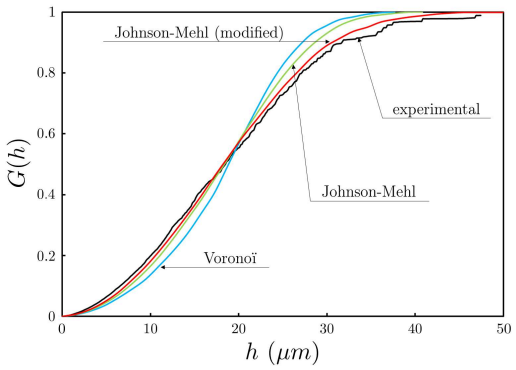

Fig. 4. 2D grain size distributions. Black: measured in Fig. 3. Light blue, green, red: Voronoi, Johnson-Mehl and modified Johnson-Mehl models respectively.

Thermoelastic behavior for constituents

The TATB crystal lattice is triclinic[8], with two molecules per unit cell. The unit cell parameters are $a = 9.01$ Å, $b = 9.028$ Å, $c = 6.812$ Å, $\alpha = 108.59°$, $\beta = 91.82°$ and $\gamma = 119.97°$. The crystal is made of $(\mathbf{a}, \mathbf{b})$ plane layers of hydrogen-bonded TATB molecules, stacked together by weaker van der Waals bonds.

Bedrov et al[9] have calculated its 21 independent elastic constants at room temperature and pressure using an atomistic approach. They are listed in Table 1, in a direct reference frame $(\mathbf{e}_1, \mathbf{e}_2, \mathbf{e}_3)$ such that $\mathbf{e}_1$ is aligned with $\mathbf{a}$, and $\mathbf{e}_2$ lies in the $(\mathbf{a}, \mathbf{b})$ plane. The 6 components of the thermal expansion tensor, listed in Table 2, are computed in the same reference frame from the X-ray diffraction data of Kolb et al[5].

The grains will be assumed to be randomly oriented in the tessellation of Fig. 5. Each grain will therefore be associated with a rotation tensor $\mathbf{R}$ linking its crystallographic orientation to the fixed laboratory reference frame. Its elastic and thermal expansion tensors are then expressed in the latter by

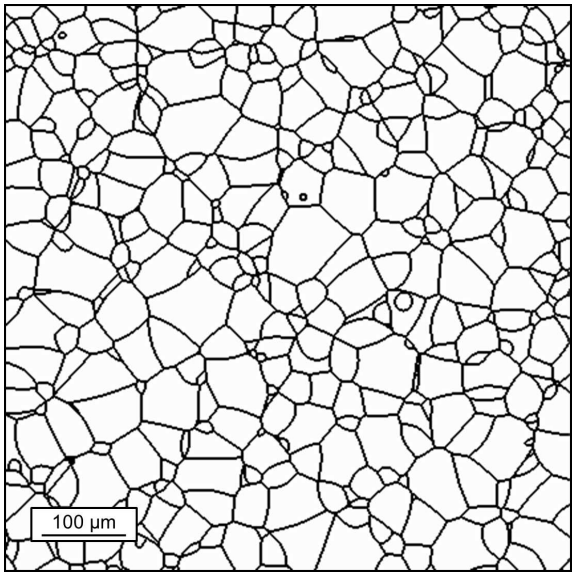

Fig. 5. A 2D slice of the modified Johnson-Mehl tessellation (same scale as in Fig. 3).

Table 1. Elastic tensor components (from Bedrov et al.[9], in GPa), standard Voigt notations.

C_{11}	65.7	C_{13}	4.0	C_{26}	1.0
C_{22}	62.0	C_{23}	5.0	C_{34}	0.2
C_{33}	18.3	C_{14}	-0.2	C_{35}	-0.4
C_{44}	1.4	C_{15}	-1.0	C_{36}	-0.4
C_{55}	0.68	C_{16}	1.0	C_{45}	0.1
C_{66}	21.6	C_{24}	0.6	C_{46}	0.3
C_{12}	18.5	C_{25}	-0.5	C_{56}	0.4

the following expressions:

$$\begin{aligned} C_{IJKL} =& R^T_{Ii} R^T_{Jj} C_{ijkl} R_{kK} R_{lL} \\ \alpha_{IJ} =& R^T_{Ii} \alpha_{ij} R_{jJ} \end{aligned} \tag{2}$$

where upper case indices are relative to the fixed laboratory frame, lower ones to the local crystallographic reference frame, and R^T_{Ii} stands for the transpose of R_{iI}.

The FFT computational method

The homogenization tool developed here consists in applying a macroscopic load to a volume element representative of the studied microstructure, computing the local thermomechanical fields, and deriving the overall response. Being relatively less demanding than the finite element method and requiring no meshing, the FFT-based numerical scheme is chosen. Its principle, first proposed by Moulinec and Suquet[10] for numerical homogenization under periodic boundary conditions, will only be outlined here.

Table 2. Thermal expansion tensor components (computed from the data of Kolb et al.[5], in K^{-1}), standard tensorial notations.

α_{11}	8.28×10^{-6}	α_{12}	3.34×10^{-6}
α_{13}	0.41×10^{-6}	α_{22}	29.04×10^{-6}
α_{23}	-26.14×10^{-6}	α_{33}	264.28×10^{-6}

For periodic homogenization, it can be shown that the macroscopic strain (resp. stress) is the spatial average of the microscopic strain (resp. stress) field. Therefore, applying a macroscopic load is equivalent to prescribing its spatial average, and the method consists in determining the local field fluctuations. Uniform temperature fields will be assumed in the sequel.

The problem statement is the following:

$$\begin{aligned} \sigma_{ij,j} =& 0 \\ \varepsilon_{kl} =& \frac{1}{2}\left(u_{k,l} + u_{l,k}\right) \\ \sigma_{ij}(x) =& C_{ijkl}(x)\left[\varepsilon_{kl}(x) - \alpha_{kl}(x)\Delta T\right] \end{aligned} \tag{3}$$

where σ is the stress tensor, ε the strain tensor, $\mathbf{u}$ the displacement vector, and $\mathbb{C}$ and α are the elastic and thermal expansion tensors defined in Tables 1 and 2 respectively. The set of equations (3) is complemented by periodic displacement fluctuations or anti-periodic traction fluctuations boundary conditions.

This problem can be replaced by the equivalent problem of a homogeneous elastic medium of stiffness tensor $\mathbb{C}^0$ submitted to the same boundary conditions, but pre-loaded by a "polarization" stress field τ, given by:

$$\tau_{ij} = \sigma_{ij} - C^0_{ijkl} : \varepsilon_{kl} \tag{4}$$

The solution of this problem is given by the Lippman-Schwinger equation:

$$\varepsilon = \bar{\varepsilon} - \mathbb{G}^0 \star \tau \tag{5}$$

in which $\mathbb{G}^0$ is the Green operator associated with $\mathbb{C}^0$, $\bar{\varepsilon}$ is the non-fluctuating part of the strain field

(macroscopic strain tensor), and the symbol $\star$ stands for the convolution product.

This implicit equation is solved iteratively using the high convergence rate scheme proposed by Eyre and Milton[11], adapted to the thermoelastic case. The strain field is initialized to the macroscopic value. The stress field is then computed using Eqn. $(3)_3$, as well as polarization stresses using Eqn. (4). Eqn. (5) is then evaluated in the Fourier space, which has the advantage of transforming the convolution product into a simple algebraic product, and yields a new evaluation of the strain field. This recursive loop ends up when the strain field attains a stationary value, within a prescribed accuracy.

Results

The first aim of the method is to predict (linear thermoelastic) macroscopic properties.This is done by performing 7 computations, each one prescribing independent applied macroscopic strains and temperature. The elastic moduli and the components of the thermal expansion tensor are then calculated by averaging over the stress tensor fields.

However, these macroscopic moduli are necessarily evaluated on finite volumes, and are therefore subject to statistical fluctuations. In order to evaluate the size of the representative volume element (RVE) needed to achieve a reasonable accuracy for macroscopic moduli, the computations are performed on a relatively large volume of 1024^3 voxels (about 12,000 grains, 804^3 µm^3). The averaging procedure is then conducted on non overlapping sub-volumes of decreasing sizes. From these data, the statistical variance (i.e. the accuracy) of the averages (and thus of the macroscopic properties) can be related to the size of the sub-volumes.

The predicted behavior is very nearly isotropic, as expected, given the random nature of the microstructure and crystallographic orientations. For the 1024^3 voxel volume, we obtain a bulk modulus of 17.2±0.1 GPa, a shear modulus of 7.4±0.04 GPa (Young's modulus: 19.3 GPa, Poisson's coefficient: 0.312), and a volumetric thermal expansion coefficient of $2.50\times10^{-4} \pm 0.06\times10^{-4}$ K^{-1}. It appears clearly that the thermal expansion coefficient is less accurately predicted than the elastic moduli.

Conversely, it could be determined that an accuracy of 0.1% on the bulk and the shear moduli needs a representative volume element of 2.5^3 mm^3 (about 38,000 grains, 3250^3 voxels), and of 6.2^3 mm^3 for the thermal expansion coefficient. As a rule, it was shown that the linear size of the representative volume element must be increased by a factor 4.6 to increase the accuracy of the macroscopic properties by an order of magnitude.

Local field fluctuations are illustrated by Figs. 6 and 7. In Fig. 6, a macroscopic temperature increase of 1 K is prescribed, all macroscopic strains being kept to zero. Therefore, Fig. 6 displays the local strains per degree.

Longitudinal strains fluctuate strongly. Since zero strains are prescribed, stresses must be predominantly compressive. Despite this, tensile (in blue) strains develop. Very strong gradients are also noticed at most grain boundaries, suggesting that debonding might occur for sufficient thermal loading.

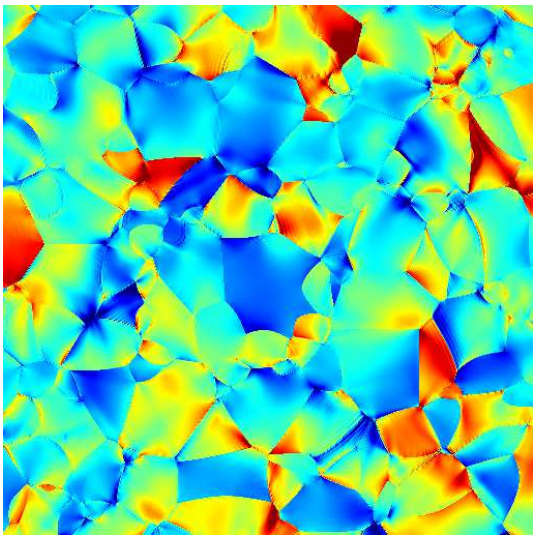

Fig. 6. Longitudinal strain field ε_{11}. Applied strain: $\bar{\varepsilon}_{ij} = 0$; applied temp. increase: $\Delta T = 1$ K. Min. (blue): -5.0×10^{-5}. Max. (red): 4.7×10^{-5}. The 1 direction is vertical on the map.

In Fig. 7, a macroscopic longitudinal strain of 1 is prescribed while maintaining the temperature constant. Therefore, Fig. 7 displays the local strain fields normalized with respect to the applied strain.

Longitudinal strains also fluctuate strongly. Val-

ues as high as three times the mean strain are recorded. In this case, intra-granular fluctuations are larger than for thermal loading, while strain gradients appear somewhat weaker at grain boundaries. This might suggest intra-granular cracking rather than debonding under mechanical loads.

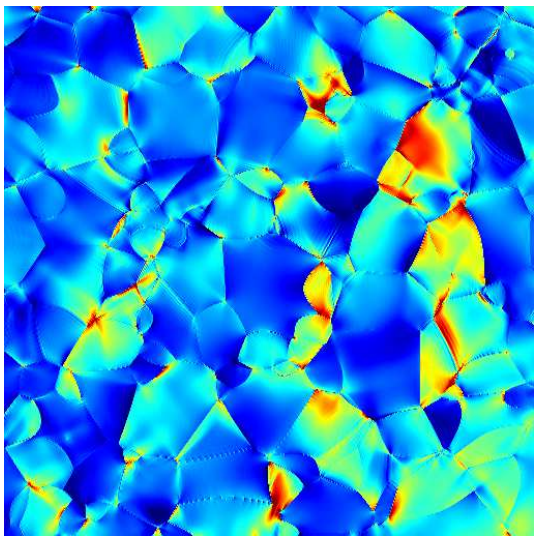

Fig. 7. Longitudinal strain field ε_{11}. Applied longitudinal strain: $\bar{\varepsilon}_{11} = 1$, other components are zero; applied temp. increase: $\Delta T = 0$. Min. (blue): 0.09. Max. (red): 2.96. The 1 direction is vertical on the map.

Discussion

The macroscopic elastic properties predicted for the polycrystal are quite far from actual values measured on the real material. Schapery[12] has given theoretical bounds for the volumetric thermal expansion coefficient of polycrystals (Fig. 8). It appears that the value predicted by FFT computations lies within the bounds. This suggests that the computational method is not defective, and that the origin of overestimations has to be sought elsewhere.

Fig. 2 shows that the volumetric thermal expansion coefficient increases dramatically above the glass transition temperature, suggesting that the binder plays a strong role on internal stresses buildup and ultimately on the value of the volumetric thermal expansion coefficient. In order to evaluate the potential role of the binder, the grain boundaries were replaced by a 4 voxel wide interphase with isotropic thermoelastic properties (Young's modulus: 1.77 GPa, Poisson's coefficient: 0.32, volumetric thermal expansion coefficient: 0). The real binder properties being unknown at present, these properties are chosen to be of the magnitude order of that of usual amorphous polymers with comparable glass transition temperature.

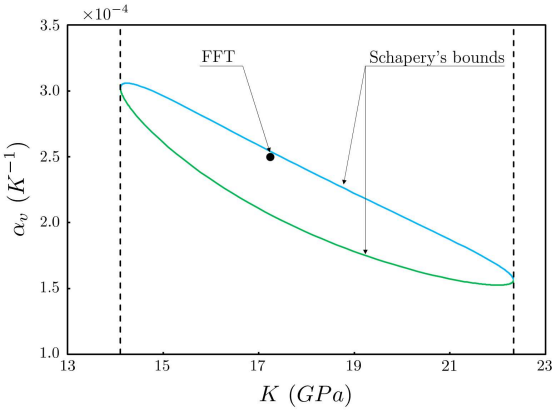

Fig. 8. Schapery[12] theoretical bounds for the volumetric thermal expansion coefficient of the polycrystal. The vertical lines are Hill's bounds[13] for the bulk modulus.

The role of the binder is illustrated in Fig. 9, to be compared to that of Fig. 6, relative to the case without binder. A more quantitative insight is provided by the field histograms given in Fig. 10. Globally, stresses are higher in the crystals than in the binder. This is especially true for the mean stress average, approximately twice as high in the crystals than in the binder.

The computations yield again an isotropic macroscopic response, with a Young's modulus of 8.46 GPa, a bulk modulus of 7.93 GPa, and a volumetric thermal expansion coefficient of 2.4×10^{-4} K^{-1}. Despite the crudeness of this computation, it appears clearly that the binder plays a strong softening role on the macroscopic elastic properties, not so far from experimental data, which is promising. Notice that neither porosity nor microcracks are accounted for in the present state of modeling. However, its effect on the thermal expansion coefficient is only marginal. This is not understood at present.

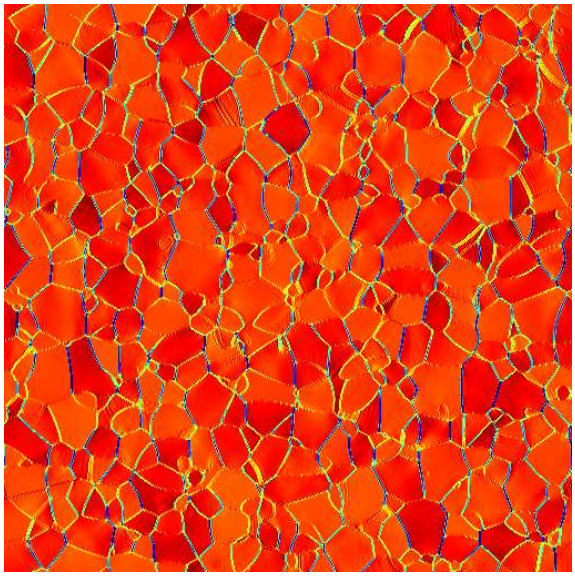

Fig. 9. Longitudinal strain field ε_{11} in polycrystal with binder. Applied thermal loading: $\Delta T = 1$; applied strain: $\overline{\varepsilon}_{ij} = 0$. Min. (blue): -8.7×10^{-4}. Max. (red): 2.0×10^{-4}. The 1 direction is vertical on the map.

Fig. 8 shows that for the polycrystal (i.e. neglecting the binder), the volumetric thermal expansion coefficient is quite sensitive to the value of the bulk modulus. To match the measured value, the bulk modulus should lie slightly above 20 GPa, which suggests that the elastic constants used in this work are somewhat underestimated.

In the recent experimental work of Stevens et al[14], the pressure-volume response of TATB powder is measured using a diamond anvil-cell apparatus, coupled with X-ray diffraction to record the evolutions of the triclinic unit-cell volume with pressure, up to 13 GPa.The authors indicate a room pressure bulk modulus above 15 GPa for the TATB single crystal, whereas the data of Bedrov et al.[9] used here yield a bulk modulus below 12 GPa. Also notice the work of Valenzano et al.[15], who obtained a partial set of elastic constants for the TATB crysta by an atomistic approach. They indicate a value of C_{11}, one of the main contributions to the bulk modulus, 20% higher than that of Bedrov et al[9]. It is therefore likely that the values used here for the elastic constants are the main source of inaccuracies.

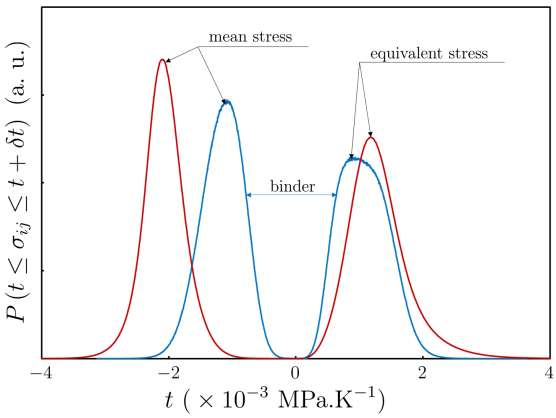

Fig. 10. Mean and equivalent stress histograms related to Fig. 9. Each histogram is normalized such that $\int_{-\infty}^{+\infty} P(t)dt = 1$. Blue: in the binder; red: in the crystals.

Conclusion and future work

The work presented here has demonstrated that it is possible to build a numerical upscaling tool with a detailed, though not yet fully realistic, description of the microstructure. The first results have shown that input data are of the utmost importance, especially the anisotropic elastic constants for the TATB crystal.

The next tasks will be to improve the virtual microstructure model, which should incorporate the elongated character of the grains, their (sometimes strongly) non-convex forms, and ultimately the presence of vestigial prills.

The behavior of the binder is being characterized at present, at least in the glassy domain, i.e. below the glass transition temperature. An elastic-plastic constitutive model will be incorporated in the method. Besides it is planned to perform real-time observations at the microstructure level during a quasi-static compression experiment, in order to get data for validation purposes.

Future work should extend the method by accounting for grain microcracking and plasticity, and for grain-binder debonding, in order to evaluate the effects of each potential mesoscale irreversible phenomena on the macroscopic (quasi-static) response of the material.

Acknowledgments

The authors acknowledge the financial support of the French Commissariat á l'Energie Atomique. They also express their gratitude to Didier Picart and Jean-Luc Brigolle for providing macroscopic elastic constants, and to Philippe Lambert and Patrick Rey for sample preparation, optical and SEM imaging and image segmentation.

References

1. Rizzo, H. F., Humphrey, J. R. and Kolb, J. R., "Growth of 1,3,5-triamino-2,4,6-trinitrobenzene (TATB). II. Control of growth by use of high T_g binders." *Prop. Expl. Pyrotech.*, Vol. 6, pp. 27–36, 1981.

2. Maienschein, J. L. and Garcia, F., "Thermal expansion of TATB-based explosives from 300 to 566 K." *Thermochimica Acta*, Vol. 384, pp. 71–83, 2002.

3. Demol, G., Lambert, P. and Trumel, H., "A study of the microstructure of pressed TATB and its evolution after several kinds of insults." in "Proc. 11^{th} Symp. Int. on Detonation," 1998.

4. Skidmore, C. B., Phillips, D. S., Idar, D. J. and Son, S. F., "Characterizing the microstructure of selected high explosives." in "Proc. EuroPyro," 1999.

5. Kolb, J. R. and Rizzo, H. F., "Growth of 1,3,5-triamino-2,4,6-trinitrobenzene (TATB). I. Anisotropic thermal expansion." *Prop. Expl.*, Vol. 4, pp. 10–16, 1979.

6. Jeulin, D., "Random texture models for material structures." *Statistics and Computing*, Vol. 10, pp. 121–131, 2000.

7. Moller, J., "Random Johnson-Mehl tessellations." *Adv. Appl. Prob.*, Vol. 24, pp. 814–844, 1992.

8. Cady, H. H. and Larson, A. C., "The crystal structure of 1,3,5-triamino-2,4,6-trinitrobenzene." *Acta Cryst.*, Vol. 18, pp. 485–496, 1965.

9. Bedrov, D., Borodin, O., Smith, G. D., Sewell, T. D., Dattelbaum, D. M. and Stevens, L. L., "A molecular dynamics simulation study of crystalline 1,3,5-triamino-2,4,6-trinitrobenzene as a function of pressure and temperature." *J. Chem. Phys.*, Vol. 131, p. 224703, 2009.

10. Moulinec, H. and Suquet, P., "A fast numerical-method for computing the linear and nonlinear mechanical properties of the composites." *C. R. Acad. Sci.*, Vol. II 318, pp. 1417–1423, 1994.

11. Eyre, D. and Milton, G., "A fast numerical scheme for computing the response of composites using grid refinement." *Eur. J. Appl. Phys.*, Vol. 6, pp. 41–47, 1999.

12. Schapery, R. A., "Thermal expansion coefficients of composites materials based on energy principles." *Comp. Mat.*, Vol. 2, pp. 380–404, 1968.

13. Hill, R., "The elastic behaviour of a crystalline aggregate." *Proc. Phys. Soc.*, Vol. A65, pp. 349–354, 1952.

14. Stevens, L. L., Velisavljevic, N., Hooks, D. E. and Dattelbaum, D. M., "Hydrostatic Compression Curve for Triamino-Trinitrobenzene Determined to 13.0 GPa with Powder X-Ray Diffraction." *Prop. Expl. Pyrotech.*, Vol. 33, pp. 286–295, 2008.

15. Valenzano, L., Slough, W. J. and Perger, W., "Accurate prediction of second-order elastic constants from first principles: PETN and TATB." *AIP Conf. Proc.*, Vol. 1426, pp. 1191–1194, 2012.